JOURNAL OF GEOPHYSICAL RESEARCH, VOL. 117, A12303, doi:10.1029/2012JA017892, 2012

Changes in thermospheric temperature induced by high-speed solar wind streams

Larry Gardner,[1] Jan J. Sojka,[1] Robert W. Schunk,[1] and Rod Heelis[2]

Received 1 May 2012; revised 12 October 2012; accepted 15 October 2012; published 8 December 2012.

[1] During high-speed stream (HSS) events the solar wind speed increases, and the cross polar cap potential increases, leading to increased Joule heating at high latitudes. The heat input at high latitudes heats the polar regions, which then conducts to lower latitudes, producing global heating. The heating occurs during the risetime of the cross polar cap potential and throughout the period of high cross polar cap potential as seen in our simulation. These simulations are performed using the Utah State University global thermosphere model driven by Joule heating rates that are consistent with electric fields observed by DMSP-15 observations of HSS events. Cooling occurs as the cross polar cap potential decreases and continues for several days after the cross polar cap potential has returned to background values. Polar cap ionospheric observations are compared to model simulations of heating and cooling, providing evidence that the thermospheric model is capturing the HSS energy input and the post-HSS multiday return to pre-HSS conditions. The HSS heating can be as high as 100 K (as seen from both the model and the data) at high latitudes, with a corresponding, but lower, global increase in thermospheric temperature.

Citation: Gardner, L., J. J. Sojka, R. W. Schunk, and R. Heelis (2012), Changes in thermospheric temperature induced by high-speed solar wind streams, *J. Geophys. Res.*, *117*, A12303, doi:10.1029/2012JA017892.

1. Introduction

[2] During the period of low solar activity extending from 2005 to 2010 the influence of high-speed solar wind streams on the ionosphere and thermosphere has become increasingly evident [*Temmer et al.*, 2007; *Crowley et al.*, 2008; *Lei et al.*, 2008a, 2008b; *Thayer et al.*, 2008; *Mlynczak et al.*, 2008; *Tulasi Ram et al.*, 2010; *Pedatella et al.*, 2010, *Qian et al.*, 2010]. While the correlations between temporal variations in the solar wind speed and variations in thermospheric density, temperature, and ionospheric density and temperature are well established [*Lei et al.*, 2008b, 2011], the causal connections and mechanisms have not been confirmed. Recently, *Heelis and Sojka* [2011] have illustrated the correlation between the solar wind speed and the topside daytime ionospheric temperature. They hypothesize that temperature increases on the order of 100 K in the neutral atmosphere are produced by changes in the frictional heating rate that accompany changes in the polar cap potential difference. During times of solar minimum, the solar wind interplanetary magnetic field is quite weak and the polar cap potential drop is on the order of 20 kV, producing ionospheric velocities in the polar cap and the auroral zone of ~200 ms^{-1}. Increases in the solar wind speed associated with the passage of high-speed streams (HSS) may increase the potential drop to magnitudes near 60 kV, but the ability of this change to produce increases in the neutral temperature of the observed magnitude in the observed time scales has not been established. Here we seek to examine the effects that HSS induced changes in the high-latitude ionospheric convection pattern have on thermospheric temperature.

[3] To accomplish this task we utilize the thermospheric model described by *Gardner and Schunk* [2010]. The model uses the International Reference Ionosphere model [*Bilitza*, 1990] to specify the ionospheric density, composition and temperature, and the convective motion is specified by a simple description of a two-cell convection pattern at high latitudes [*Volland*, 1975]. Our purpose here is not to drive the ionosphere in a prescribed way in an attempt to reproduce a given set of observations, but to investigate the magnitude of thermospheric temperature variations that could be produced with typical changes in polar cap potential that are observed during HSS events. The temperature variations we examine include rapid initial heating, global expansion from high latitudes, and slower thermal cooling/recovery back to pre-HSS levels.

[4] To accomplish this study we use in situ observations of the polar cap potential difference as inferred from satellite (DMSP) observations. These observations are then used to parameterize a high-latitude convection pattern that drives the heating in our thermospheric model. The response to this parameterized convection pattern is then examined via the

[1]Center for Atmospheric and Space Sciences, Utah State University, Logan, Utah, USA.
[2]Hanson Center for Space Sciences, University of Texas at Dallas, Richardson, Texas, USA.

Corresponding author: L. Gardner, Center for Atmospheric and Space Sciences, Utah State University, Logan, UT 84322, USA. (larry.gardner@usu.edu)

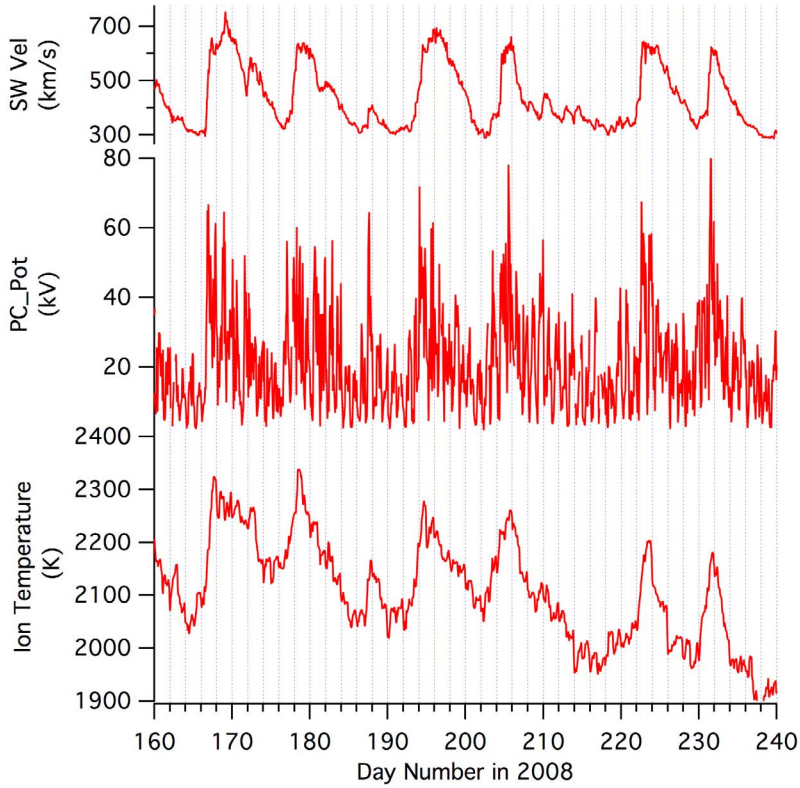

Figure 1. (top) Solar wind velocity, (middle) cross polar cap potential, and (bottom) ion temperature at 30° magnetic latitude in the morning sector as observed by the ACE and DMSP satellites for days 160 through 240 in 2008, showing oscillations due to high-speed streams.

simulated HSS event, where a multiday neutral temperature response is compared to ionospheric observations at high and auroral latitudes. A caveat to this comparison is that an effort is made to compare a "generic" thermospheric response with a "generic" ionospheric response but from cases that are separated by 1 year and 2 days.

[5] This paper proceeds as follows. Section 2 describes the DMSP satellite HSS events used to define the frictional heating input while section 3 provides a description of the thermospheric response. Ground-based ISR observations are compared to the thermospheric simulations in section 4, and discussion of the assumptions and inferences of this study are given in section 5 with conclusions given in section 6.

2. DMSP Satellite Observations of HSS

[6] The Defense Meteorological Satellite Program (DMSP) satellites are approximately in sun synchronous orbits at altitudes near 830 km. These satellites nominally lie in fixed local time planes with equatorial crossing times near 0630, 0930, 1830, and 2130. The high inclination (98°) of the satellites is such that they cross the magnetic polar regions almost every orbit, and their orbital period of about 100 min results in 14.4 orbits per day. Each satellite has a suite of environmental/science instruments, with the local plasma environment sensor package, SSIES, providing measurements of the ion number density, ion composition, ion temperature and ion drift velocity [*Rich and Hairston*, 1994]. During the 2008 period for this study, the F15 orbit was approximately parallel to the dawn-dusk meridian, having precessed to this location since launch. This period was also during the extended solar minimum between solar cycles 23 and 24, where geospace was repeatedly bombarded by coronal hole HSS, as indicated by the ACE satellite measurements of the solar wind speed. Figure 1 shows an 80 day example of these HSS events as observed by the ACE and DMSP satellites in 2008. Each enhancement begins at a pre-HSS level of 300 km/s and rapidly increases to over 500 km/s as the corotating interaction region (CIR) phase of the HSS is encountered. Two separate coronal holes generated multiple HSS events during the 80 day period shown. The first stream, due to the first coronal hole, was encountered on days 169, 196, and 223, while the second stream, due to the second coronal hole, was encountered on days 179, 206 and 232. The events for each coronal hole were separated by about 27 days, corresponding to the solar rotational period.

[7] The DMSP-F15 satellite ion drift velocity measurements made during these 80 days were analyzed to provide the electric field along dawn-dusk orbits. These were then integrated to provide the electric potential distribution across the northern hemisphere high-latitude region traversed by the satellite. For each pass the maximum potential difference along the orbit was computed, as shown in Figure 1 (middle), where it is labeled "PC_Pot," indicating the cross polar cap potential. It is important to note that the DMSP orbit, although fixed in solar local time, moves across the magnetic high latitudes from the noon sector to the nightside and back again over the course of each day. Hence, only for the passes

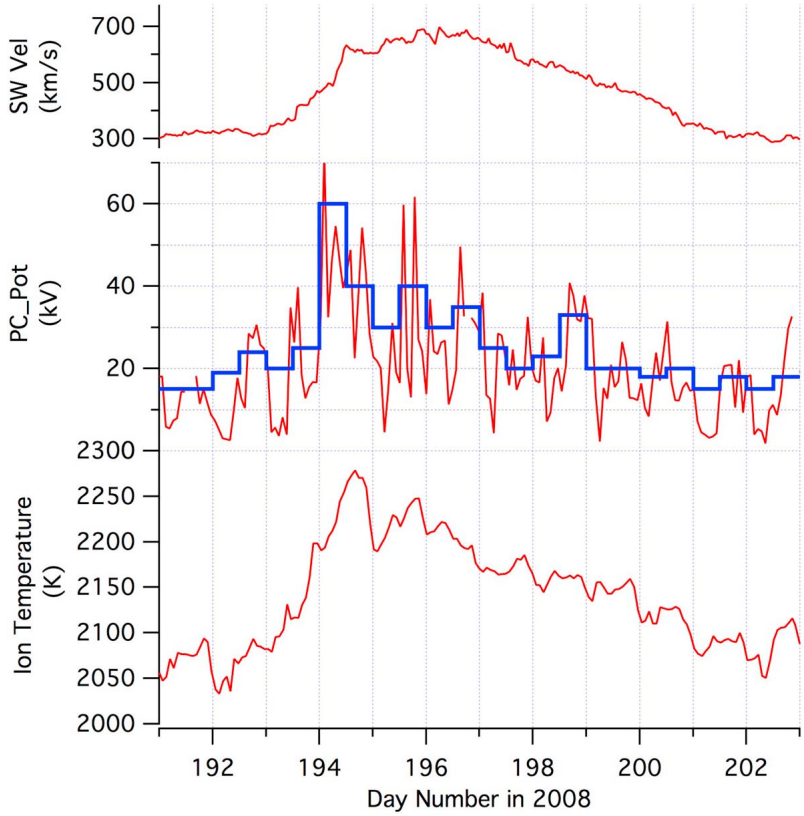

Figure 2. (top) Solar wind velocity, (middle) cross polar cap potential, with approximate 3 h estimated average, and (bottom) ion temperature at 30° magnetic latitude in the morning sector as observed by the ACE and DMSP satellites for a single high-speed steam event on days 191 through 202 in 2008.

made close to the dawn-dusk plane in the polar cap will the PC_Pot be closest to the full polar cap potential difference. In Figure 1 (middle), this orbit sweeping across the magnetic polar region is reflected in a daily variation in PC_Pot, with the upper, largest values being the most representative of the true polar cap potential difference. In addition the polar cap potential responds to changes in the interplanetary magnetic field on time scales of less than 1 h, which produces an additional level of variability in the data seen in Figure 1. Even given this variability it is clear from examination of Figure 1 (top) and Figure 1 (middle) that the polar cap potential difference is responding to the HSS. Prior to the HSS arrival the polar cap potential difference is about 20 KV, it then rapidly increases into the 50 to 60 KV range, from which it then decreases slowly over 1 to 2 days. For this potential change the polar cap has not expanded significantly [cf. *Heelis and Sojka*, 2011], hence the tripling of the cross polar cap potential indicates that the electric field has tripled, which in turn increases the frictional heating rate by up to ninefold during the peak of these HSS events.

[8] The SSIES package also measures the ion temperature (Ti) at middle latitudes, shown in Figure 1 (bottom). This plot describes a plasma response in the topside ionosphere indicating an elevated Ti during the events; with maximum Ti increases typically around 200 K. Over the 80 day period of interest, which begins near summer extending toward equinox, the background Ti values also show the expected seasonal decrease.

[9] On day 188 the solar wind speed shown in Figure 1 (top), indicates a very modest increase of 50 km/s. This amount would be insufficient to cross the nominal 500 km/s HSS threshold value, hence it is not reported as an HSS. However, both the PC_Pot (Figure 1 (middle)) and Ti (Figure 1 (bottom)) plots show that the ionosphere is responding. Hence the ionosphere is driven by even weak "HSS" type fluctuations in the solar wind. In a previous study *Heelis and Sojka* [2011] show that the ion temperature increase occurs throughout the middle latitude ionosphere in a region where the plasma velocity is very small and thus in situ frictional heating cannot be responsible. They attribute the temperature perturbations to changes in the neutral temperature consistent with previously reported changes in thermospheric and ionospheric parameters [*Thayer et al.*, 2008; *Lei et al.*, 2008b]. While it is well established that frictional heating and particle heating will globally heat the thermosphere [*Fuller-Rowell et al.*, 1994; *Qian et al.*, 2010] in this work we wish to establish a consistency between observations of a thermospheric driver and the thermospheric response by assessing the impact of small changes in the cross polar cap potential difference as are observed during the period shown here.

[10] To study these effects we use our thermospheric model to look at the neutral temperature response to magnetospheric convection by employing a simplified two-cell ionospheric convection pattern driven primarily by the observed cross polar cap potential. Figure 2 focuses on the

period between day 191 and day 203 when an HSS occurred. In Figure 2 (top) the HSS solar wind ramp-up can be seen to take almost 2 days, from day 193 to day 195. During this ramp-up period the polar cap potential reached its maximum value early on day 194, and then slowly, over several days, decreased to its background value of 20 kV. The topside ion temperature ramps up in phase with the solar wind speed, reaching its maximum late on day 194, and then slowly decreasing to its pre-HSS value. In Figure 2 a thick line has been superimposed on the DMSP PC_Pot indicating a half-daily probable value for the cross polar cap potential that represents our best attempt to filter the variability produced by short-term variations in the solar wind driver and longer term daily variations due to the motion of the magnetic pole with respect to the spacecraft. It is this variation in the cross polar cap potential that will be mimicked in the following thermospheric model study.

3. Thermospheric Response to HSS

3.1. Global Thermosphere/Ionosphere Model

[11] Our model study of the thermospheric response to the HSS is based on a time-dependent, high-resolution model of the global thermosphere-ionosphere system [*Ma and Schunk*, 1995, 2001; *Schunk and Demars*, 2003; *Schunk et al.*, 2008]. The model calculates a simultaneous solution of the neutral gas equations of continuity, momentum, energy and mean mass, which produces global distributions of the mass density, temperature, and all three components of the neutral wind at altitudes from 90 to 500 km. The equations are solved in a spherical coordinate system fixed to the Earth using a multidimensional flux-corrected transport (FCT) technique [*Zalesak*, 1979]. The model uses an altitude, not a pressure coordinate, in the vertical direction, and nonhydrostatic equilibrium flows are allowed since the vertical velocity is solved rather than adopting the hydrostatic approximation. The spatial resolution is 2° in latitude and 3° in longitude. In the vertical direction (90–500 km), the layers are distributed nonuniformly according to the neutral gas scale height, and we use 60 layers giving a vertical resolution of ∼1 km at 100 km altitude, and ∼20 km at 500 km altitude. Migrating tides are included, and tides due to thermospheric solar forcing are calculated self-consistently in the model.

[12] Several external empirical models drive the global thermosphere model. These include the MSIS atmosphere model, the Volland electric field model, and the International Reference Ionosphere model, each of which is discussed below.

[13] The NRLMSISE-00 empirical model of the atmosphere [*Picone et al.*, 2002], which includes diurnal, semidiurnal, and terdiurnal migrating tides, was used to fix the boundary condition at 90 km. Specifically, at each time step, the neutral densities at 90 km given by the NRLMSISE-00 model were imposed as a boundary condition for the thermosphere model. As time progressed the model calculates the self-consistent winds and temperatures at 90 km as well as the thermospheric parameters above this altitude [cf. *Schunk et al.*, 2008].

[14] The magnetic field and convection electric field are treated as inputs to the thermosphere-ionosphere model. The magnetic field is calculated from a tilted dipole that rotates with the Earth [cf. *Ma and Schunk*, 1995], and the convection electric field is obtained from the empirical model of *Volland* [1975].

[15] The ionosphere affects the momentum and energy balance in the thermosphere via the ion drag and the ion-neutral frictional heating terms in the momentum and every equation respectively. For these simulations, the International Reference Ionosphere (IRI) model [*Bilitza*, 1990] was used to obtain time-dependent, global ion density distributions. In addition to the IRI background ionosphere, ionization due to auroral particle precipitation was accounted for using the method of *Roble and Ridley* [1987]. There is no feedback from the thermosphere model to the ionosphere.

[16] In addition to the frictional heating, the other major heat sources are the solar heating and the heating due to the auroral particle precipitation. The solar heating includes the heating due to the solar EUV and the Schumann-Runge continuum. The solar EUV heating rate is calculated based on the expression given by *Schunk* [1988]. The heating rate for the Schumann-Runge continuum is calculated in a similar way based on the tables given by *Torr et al.* [1980]. The heating rate due to the auroral particle precipitation is calculated from the formulation of *Roble and Ridley* [1987]. For a detailed formulation of the heating and cooling processes, see *Ma and Schunk* [1995].

[17] Our global thermosphere-ionosphere model can account for large-scale redistribution of energy and momentum in the thermosphere. Most recently, the model has been used to study the generation of Traveling Atmospheric Disturbances during pulsating geomagnetic storms [*Gardner and Schunk*, 2010], and the impact that an upward propagating large-scale gravity wave has on the thermosphere [*Gardner and Schunk*, 2011].

3.2. The HSS Thermosphere Driver

[18] Figure 2 provided guidance for selecting an input to the Volland two-cell ionospheric convection model. We emphasize again that this is not a case study, but rather an exploration of how the HSS low levels of disturbed geomagnetic activity are reflected in a global response of the thermosphere. The red line in Figure 3 reproduces the Figure 2 PC_Pot average value, while the blue line represents a simplified cross-tail potential evolution used in the following study. This temporal variation of the cross polar cap potential is used to adjust the Volland two-cell convection pattern. The convection cells remain symmetric with only a very small expansion of the polar cap. Hence, during the disturbed period, the ionospheric convection speed is distributed equally in the dawn and dusk sectors. We emphasize that that we are interested in the magnitude of the perturbations that can be produced by this modest change in the cross polar cap potential over a period of several days, and thus we can change the cross polar cap potential over a period of a few hours with no significant impact on the subsequent evolution on time scales of a few days.

[19] In addition to the frictional heating the auroral input is obtained from the method of *Roble and Ridley* [1987]. The method of *Roble and Ridley* [1987] uses an analytic expression for the auroral oval. The oval is centered on the magnetic pole, with half widths for the sunward and antisunward maximum and minimum values of the oval width, characteristic energy of the precipitating particles, and the energy flux being specified. For a detailed explanation, see *Ma and*

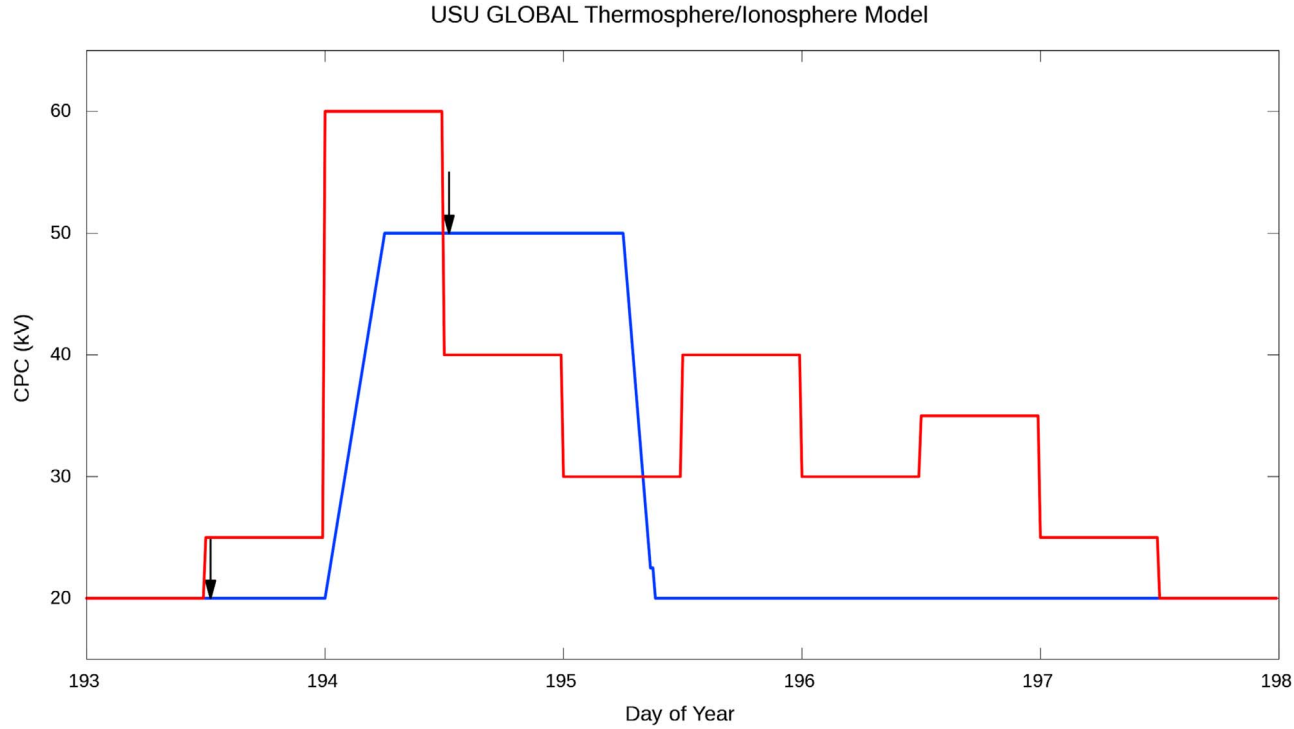

Figure 3. The half-day assessed cross tail potential for days 193 through 197 (red line) and the simplified cross tail potential input used to drive a symmetric Volland two-cell convection pattern (blue line).

Schunk [1995] Appendix C. In general the auroral precipitation contributes no more than 20% of the energy deposited in storms. Therefore, the use of *Roble and Ridley* [1987] is acceptable since the majority of frictional heating (80%) comes from polar cap flows due to the cross polar cap potential.

[20] Figure 4 shows two dial plots, corresponding to the times of the black arrows in Figure 3, for the two extremes of

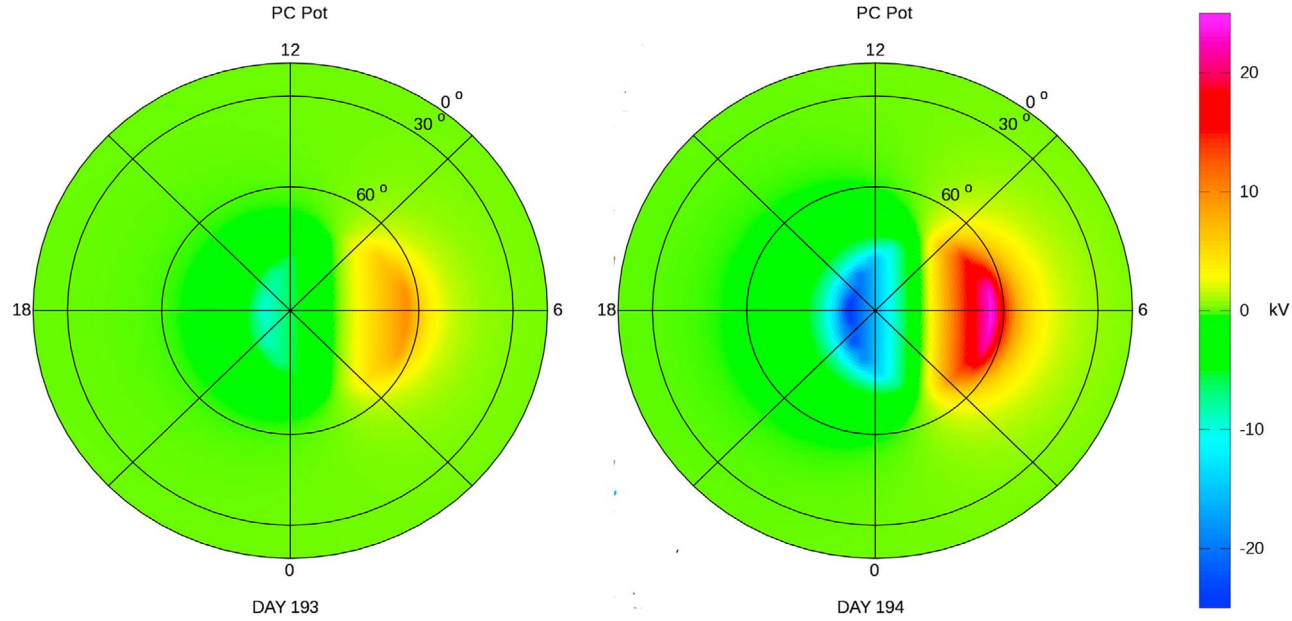

Figure 4. Volland potential pattern for quiet conditions (left) represented by day 193 and (right) for the peak in the simulated potential. The potential is color-coded in a geographic polar diagram, with local noon at the top.

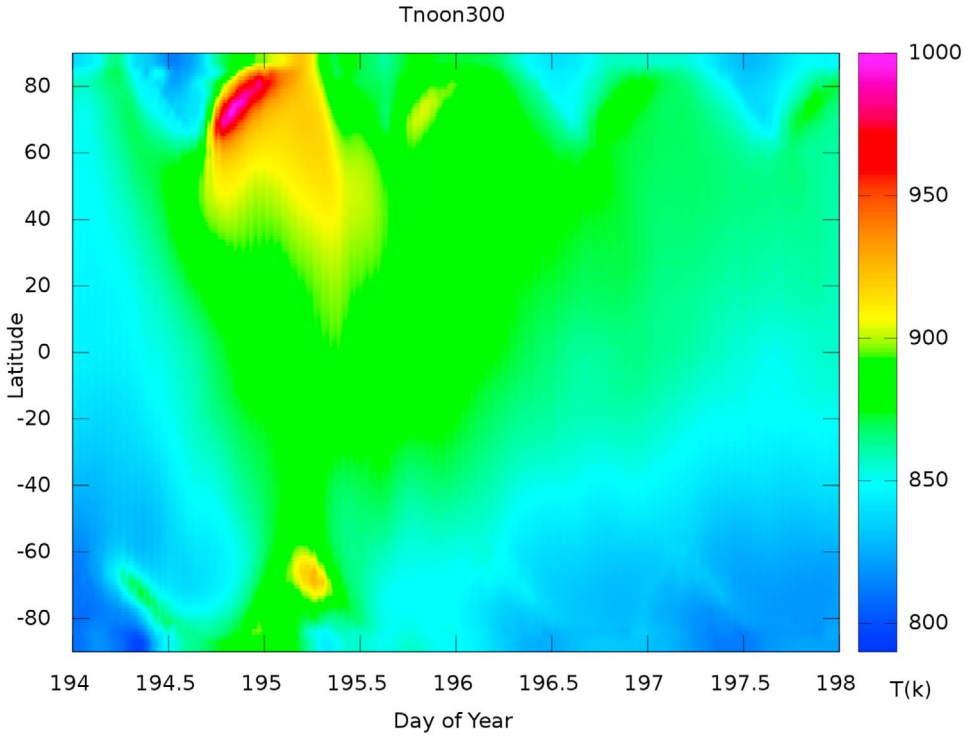

Figure 5. Plot showing the evolution of the modeled Tn at 300 km along the noon geographic meridian. The temperature is displayed in a linear color scale extending from 790 to 1000 km, and the latitude extent is from −90° to 90° geographic latitude.

the cross polar cap potential. Figure 4 (left) is at noon on day 193 when the cross polar cap potential is at its minimum value. Figure 4 (right) is at noon on day 194 and is representative of all background (20 kV) values. At each time in the simulation the cross polar cap potential (blue line in Figure 2) is used to adjust the Volland ionospheric convection pattern at high latitudes.

3.3. Thermosphere Simulation of Response to Idealized HSS

[21] The simulation begins on day 193 with a suitable equilibrium thermosphere for the corresponding quiet geomagnetic and solar conditions. Then the simulation proceeds using the Volland two-cell driver described in the previous section. During the HSS period, beginning on day 194 at 0000 UT and ending on day 195 at 1000 UT frictional heating is driving the thermosphere. The results of this heating cause the thermospheric temperature to increase and, over a longer time period, cool back to the pre-HSS conditions.

[22] Figure 5 shows the evolution of the neutral temperature at 300 km along the local noon meridian. The HSS frictional heating begins at 0000 UT on day 194 and the electric field reaches its peak at 0600 UT, which is then maintained until 0600 UT on day 195. The neutral temperature indicates high-latitude heating early on day 194 but its peak values occur later on day 194 when the cross polar cap potential is at its maximum. The two hemispheres, although driven by the same convection electric field, respond differently. This is caused by the seasonal difference in the two hemispheres with summer in the north and winter in the south. Globally, an overall heating of at least 50 K occurs even at the equator. At the higher latitudes, especially in the northern hemisphere, the heating leads to temperatures that are elevated by nearly 200 K in the auroral regions with maximum increases of 100 to 150 K at middle latitudes. By day 198 0000 UT, 2.5 days after the HSS energy input ended, the temperatures are returning to their pre-HSS levels.

[23] At other local times the HSS evolution is less dramatic but follows a similar trend. The neutral temperature evolution at 300 km for a local time of 1800 h (dusk) is shown in Figure 6. In this local time sector the temperature enhancement is less and also its maximum is located in the northern polar cap where the maximum difference between the ion and neutral velocities is expected. This is shown by the high-temperature spot above 80° north latitude just after the start of day 195.

4. Observations and Model Comparisons

4.1. Incoherent Scatter Radar Campaign

[24] During the International Polar Year (IPY) beginning on 1 March 2007 an ongoing incoherent scatter radar (ISR) campaign was run with coordination between the major ISRs. Of specific interest to this study were the observations made by two ISRs that operated on a 24/7 schedule during the IPY. The EISCAT Svalbard Radar (ESR) located at 78°9′N, 16°12′E and the Poker Flat Incoherent Scatter Radar (PFISR) located at 66°8′N, 212°32′E were both configured to operate continuously on a low duty cycle for the entire IPY [*Sojka et al.*, 2007]. Each ISR observed the ionospheric *E* and *F* region plasma along the local magnetic field-line with a cadence usually better than 15 min [*Sojka et al.*, 2009a, 2009b]. At

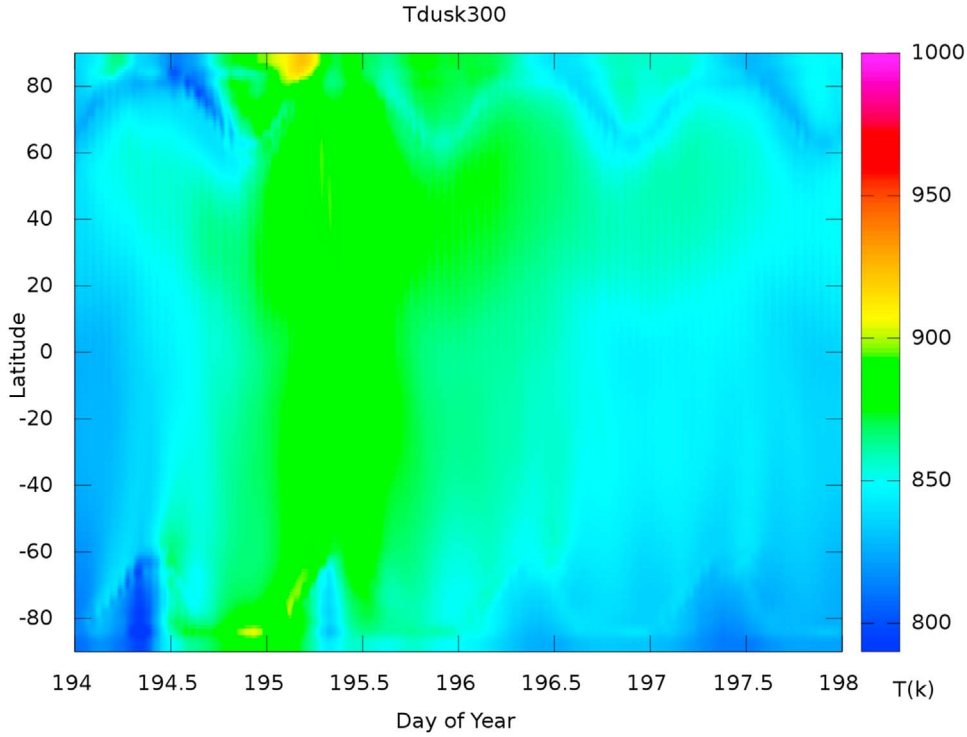

Figure 6. Same as Figure 5, but for the 1800 solar local time meridian Tn evolution. This figure has the same dynamic range for Tn as in Figure 5.

both locations almost one month of data was missing due to technical reasons. At ESR the local Svalbard power station was off-line for almost a month, and at PFISR a month was missed during construction as the last 10% of the antenna system was installed. During the rest of the year about 85% of the target 24/7 operations was achieved. This campaign provided extremely high temporal resolution sampling of key ionospheric parameters in the polar cap (ESR) and auroral zone (PFISR) for periods spanning many solar rotations. This long duration campaign enables monitoring of the recurrent HSS-CIR impacts on the ionosphere from the same source coronal hole over many solar rotations.

[25] Both PFISR and ESR observed the ionosphere's response to many of the same HSS, but these were all before the day 193, 2008 study shown in sections 2 and 3. However, 1 year earlier in 2007 both ISRs observed the response to an HSS that occurred on day 195 in 2007. The seasonal conditions were similar, as was the solar activity as defined by the 10.7 cm radio solar flux index. Hence in sections 4.1 and 4.2 the thermospheric study from section 3 will be compared in only a broadly quantitative sense with the PFISR and ESR observations.

[26] One thing to note for this simulation is that the data for the HSS were for day 194, 2008, while the data from the radar measurements were for day 195, 2007. Therefore, there is an offset of about 1 day and 1 year between the HSS event that is simulated, and the radar data that is used to compare to the model results. The reason for this offset was the lack of radar data for the 2008 period, where the HSS data were taken. Since the solar conditions were similar for the 2007 and 2008 periods, the radar data from 2007 is used to compare to the model results. Even with this offset the morphologies are very similar, and this is what this paper is looking into.

4.2. Model-PFISR Comparison

[27] The PFISR observations of ion temperature at 300 km are shown in Figure 7 (bottom) as the black line between day 194 and 201, 2007. Each day, the station undergoes a systematic solar zenith angle–local time variation. This is most clearly seen from day 198 to day 201. The mild diurnal modulation is readily compared with the red line representing the thermospheric model quiet day variation of neutral temperature. Over those 2 to 3 days the times for the maximum and minimum in the observed ion temperature and modeled neutral temperature appear to coincide. The model values are $\sim$25 K hotter than the measurements, and the observations have a $\pm$25 K noise variability due primarily to the analysis of a relatively weak radar return signal. Although it is clear that the neutral temperature cannot be higher than the ion temperature, no attempt to recalibrate the model to remove the small difference has been undertaken. Note that in the thermosphere-ionosphere model we compute only the neutral temperature. However, at 300 km which is near but above the F layer peak, the ion temperature should be mainly in thermal equilibrium with the neutral temperature. Under strong frictional heating conditions it is known that the ion temperature itself will be elevated well beyond the heated neutral gas. We return to this discussion later in this section and in section 4.3.

[28] On day 195, PFISR detected a sudden increase in Ti from a quiet level of about 800 K to values above 1200 K.

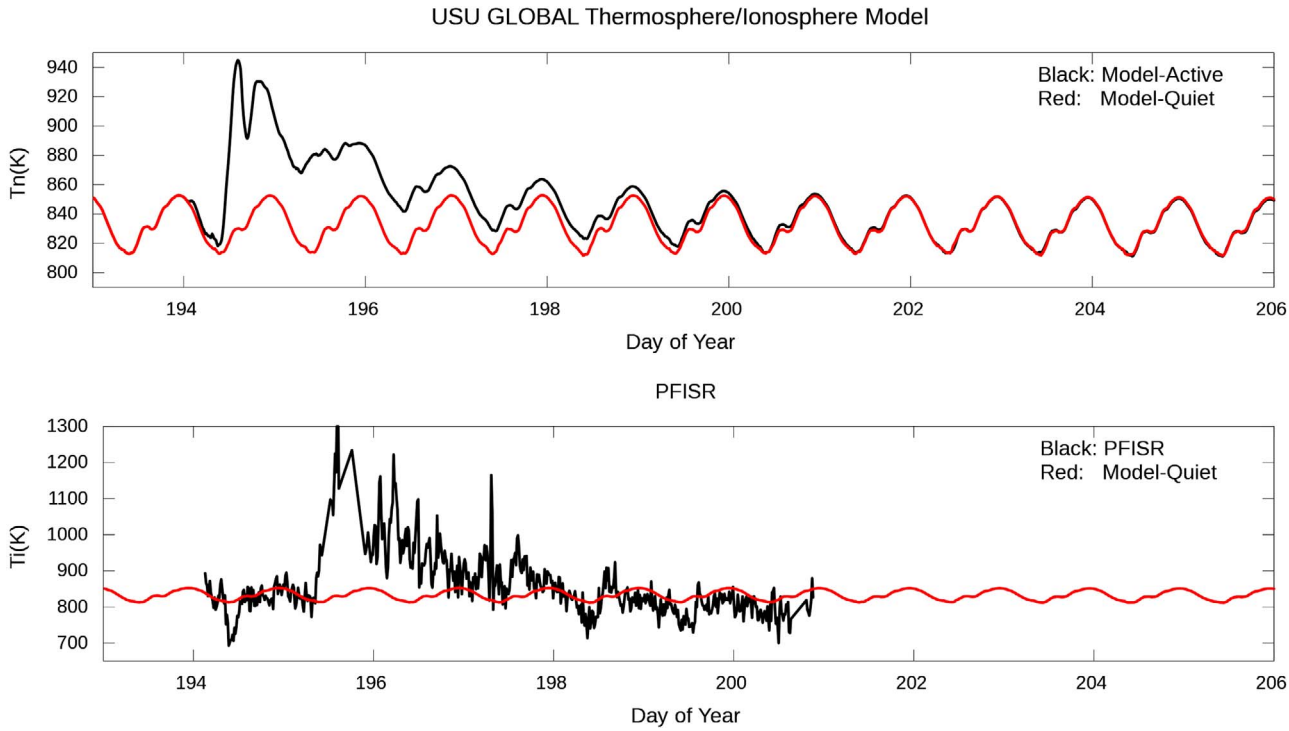

Figure 7. (top) Tn at 300 km modeled by the thermosphere model and (bottom) Ti at 300 km observed by PFISR in 2007 for similar season and solar activity conditions. In each panel the red line represents Tn at 300 km for ongoing quiet geomagnetic conditions, and the black line represents the model results (Figure 7 (top)) or PFISR measurements (Figure 7 (bottom)).

This enhanced Ti continued for several days. The risetime took ~6 h and then the recovery to preenhanced conditions took a further 2.5 days. This entire enhancement was associated with a HSS with similar characteristics to those described in section 2 and modeled in section 3. The observed enhancements are also associated with fluctuations of many 100 s of K that appear on time scales of a few hours, the upper envelope of which represents impulsive frictional heating. These fluctuations are not the quiet time noise fluctuations but rather are systematic changes in Ti as it responds to changes/variability in the electric field. From about day 196, 00:00 UT to about day 197, 12:00 UT the variability has an upper and lower envelope. The lower envelope is of particular interest, and represents the coldest level that could be assumed to be close to, if not exactly equal to, the thermospheric neutral temperature. The upper envelope represents the impulsive frictional ion heating caused by enhancements in the local electric field. This upper envelope is many hundreds of degrees hotter than the background Ti as well as the neutral temperature. The lower envelope represents a probable upper limit to the expected heated neutral temperature at 300 km.

[29] Figure 7 (top) compares the modeled neutral temperature response at the PFISR location to the simulated HSS (black line). Recall the simulation was carried out for a HSS observed by DMSP on day 193, 2008 while IPY occurred the year prior. The neutral temperature response begins with a rapid enhancement from 830 K to just over 920 K that occurs in a few hours. Its recovery to the pre-HSS temperatures takes at least 3 days. This time is estimated from a comparison with the quiet time neutral temperature at 300 km shown as a red line. In comparing with the PFISR observations it is important to compare the model with the lower envelope of the PFISR ion temperature variations. In this case the 100 K increase in neutral temperature (Tn) is comparable to the ~150 K increase in Ti based on the projection of the lower envelope of the Ti variability in Figure 7 (bottom). It is apparent from this comparison of model results and observations near the equatorward edges of the auroral zone that perturbations in the neutral temperature of ~100 K can be produced by increases in the convection electric field associated with HSS.

4.3. Model-ESR Comparison

[30] The ESR is located at Svalbard and is for most geomagnetic conditions a polar cap observatory, and around noon it becomes a cusp station. Observations made from the DMSP satellite, described earlier suggest that the polar cap size did not increase appreciably, but the electric field almost triples during the HSS passage. Hence, ESR located in the polar cap should respond similarly, if not more strongly, than the auroral station PFISR.

[31] Figure 8 addresses this hypothesis by showing ESR ion temperature observations at 300 km and the corresponding model neutral temperature. The same number of days as used for the PFISR data if Figure 7 were used for ESR data in Figure 8. The observed ion temperature for quiet day 194, and post-HSS quiet days 199 and 200 has the same characteristics as the quiet time neutral temperature but with a ±25 K variability. The maximum ESR Ti enhancements reach temperatures significantly larger than 1300 K. This is noticeably higher than those found at PFISR (Figure 7). Figure 7 (top)

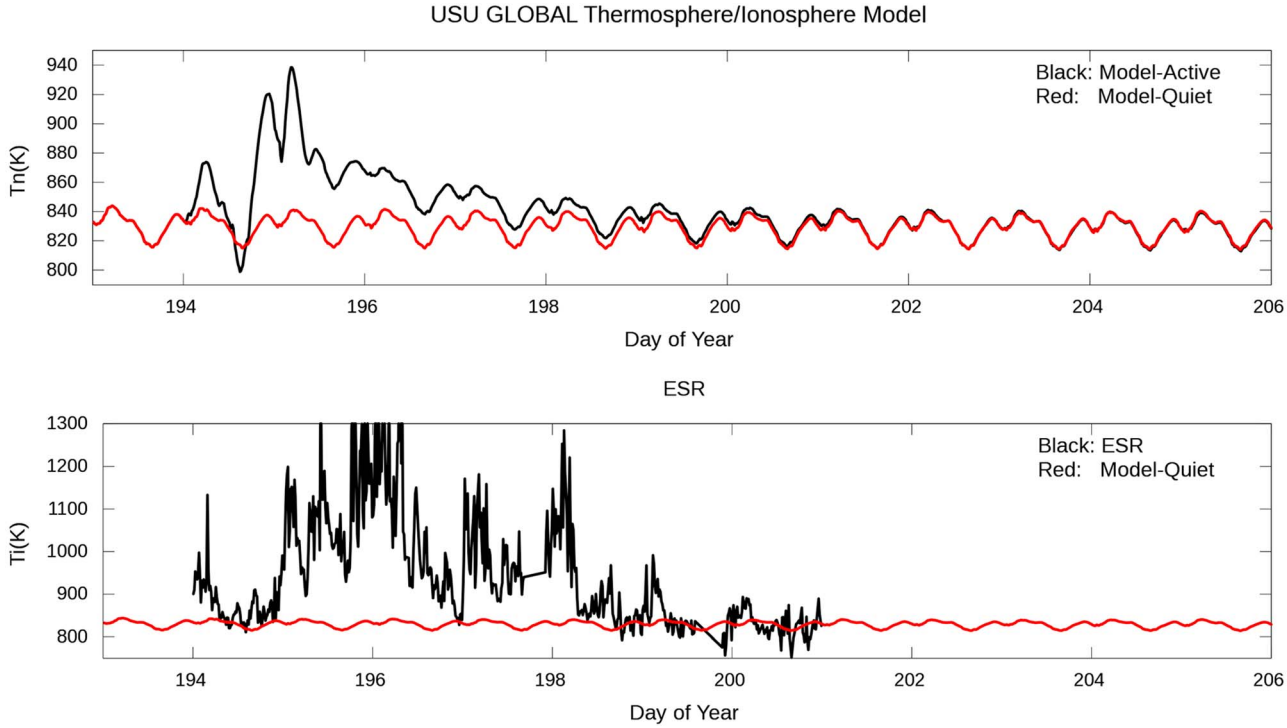

Figure 8. Same as Figure 7, but for the ESR measurements.

showing the neutral temperature for the ESR location (Figure 8) reaches 940 K, which is similar to the PFISR maximum value of 940 K. Between day 195, 00:00 UT and 199, 00:00 UT the lowest ion temperatures are typically more than 100 K above the quiet time values. On day 197 00:00 UT there is a period of a few hours when the Ti value does drop almost to the background value but then increases again for a further day and a half. The enhanced Ti observed at ESR is quite complex, with an additional strong diurnal modulation. The overall similarity between the two sites in comparing the observed Ti and model Tn is still very evident.

5. Discussion

[32] The study brings together observations from 2007 and 2008, specifically ISR observations in the polar and auroral regions in 2007 and from a DMSP satellite in 2008. However, the solar radio flux conditions for both periods are similar. This implies that the solar UV-EUV conditions, which are a key input to the dayside thermosphere and ionosphere, are identical. During both periods the geomagnetic conditions reflected the recurrence of the HSS, with a temporal envelope that is also very similar in both periods. The HSS events, although not expected to be identical for events separated by a year, are in an overall sense, a very repeatable phenomena whose long duration, 2 to 3 days, makes them unique geomagnetic drivers. It is this property that we use to justify our study that compares HSS simulations with observations that are separated by 1 year.

[33] In this study we compare the thermospheric temperature, Tn, with ionospheric ion temperatures, Ti, at an altitude of 300 km. This choice is based on the realization that the HSS heating changes slowly over several days, hence allowing the thermosphere to come into pseudo equilibrium with the heat source. Typical time scales for the thermospheric thermal response at solar minimum are hours to several hours in contrast to the HSS passage, which takes days. Based on this argument the thermospheric temperature shows a multiday heating and cooling profile. The maximum exospheric temperature, as simulated, is 100 to 150 K warmer than the pre-HSS condition. At solar minimum, an altitude of 300 km is a reasonable location for Tn having reached its exospheric temperature. At this altitude most of the time the ions will be near thermal equilibrium with the neutrals. The thermal coupling of the ions to the electron gas, which is usually hotter, would at this altitude be weak. During specific periods of impulsive, large electric fields, frictional heating leads to ion temperatures many hundreds of degrees hotter than the neutrals. However, once the impulsive field diminishes, the ions will thermalize back to the neutral temperature in a few minutes or less. These arguments lead us to believe that during the HSS when the thermosphere has become heated by 100–150 K the coldest temperatures the ions can have will also reflect this 100–150 K heating. Our ISR observations at both PFISR and ESR indicate a possibly higher level of heating, 100–250 K. However, the overall HSS trend in both the thermosphere and ionosphere at 300 km is similar, giving further confidence to our interpretation. In the topside ionosphere near sunset, the ion cooling will also be controlled by conduction to the neutral gas, and the DMSP observations show perturbations in the ion temperature of 100 to 200 K consistent with a modulation in the neutral temperature.

6. Conclusion

[34] This study sets out to quantify the argument that during HSS passage, enhanced high-latitude convection is

sufficient to heat the thermosphere, not just at high latitudes, but globally. Using DMSP-FI5 satellite observations of ionospheric convection, the magnitude of the HSS convection change is quantified in terms of the polar cap potential difference. This HSS convection is then used to drive a thermospheric model to provide the following findings: (1) The HSS input sustained for about 1 day does create high-latitude exospheric temperature increases on the order of 100 K. (2) The high-latitude thermospheric heating expands to become a global heating event. (3) Recovery of the thermosphere extends several days beyond the HSS event. (4) In both the polar cap (ESR) and auroral region (PFISR) ground-based observations of ion temperature show similar HSS heating responses both in magnitude and duration.

[35] The final comparison with the ISR observations is primarily of a qualitative nature, since the specific observations occurred in a prior year and are argued to be relevant because the HSS events over the recent solar minimum have been found to be extremely repeatable in their characteristics. However, simultaneously measured ion temperature perturbations of 100–200 K in the topside ionosphere are also consistent with the modeled increase in the neutral temperature.

[36] **Acknowledgments.** This research was support by NSF grant AGS-0962544 to USU and by NASA grants NNX07AF36G and NNX07AT82G to the University of Texas at Dallas.

[37] Robert Lysak thanks the reviewers for their assistance in evaluating this paper.

References

Bilitza, D. (Ed.) (1990), International Reference Ionosphere 1990, *Rep. NSSDC 90–22*, Natl. Space Sci. Data Cent, Greenbelt, Md.

Crowley, G., A. Reynolds, J. P. Thayer, J. Lei, L. J. Paxton, A. B. Christensen, Y. Zhang, R. R. Meier, and D. J. Strickland (2008), Periodic modulations in thermospheric composition by solar wind high speed streams, *J. Geophys. Res.*, *115*, A08314, doi:10.1029/2009JA015129.

Fuller-Rowell, T. J., M. V. Codrescu, R. J. Moffett, and S. Quegan (1994), Response of the thermosphere and ionosphere to geomagnetic storms, *J. Geophys. Res.*, *99*, 3893–3914, doi:10.1029/93JA02015.

Gardner, L. C., and R. W. Schunk (2010), Generation of traveling atmospheric disturbances during pulsating geomagnetic storms, *J. Geophys. Res.*, *115*, A08314, doi:10.1029/2009JA015129.

Gardner, L. C., and R. W. Schunk (2011), Large-scale gravity wave characteristics simulated with a high-resolution global thermosphere-ionosphere model, *J. Geophys. Res.*, *116*, A06303, doi:10.1029/2010JA015629.

Heelis, R. A., and J. J. Sojka (2011), Response of the topside ionosphere to high-speed solar wind streams, *J. Geophys. Res.*, *116*, A11314, doi:10.1029/2011JA016739.

Lei, J., J. P. Thayer, J. M. Forbes, E. K. Sutton, and R. S. Nerem (2008a), Rotating solar coronal holes and periodic modulation of the upper atmosphere, *Geophys. Res. Lett.*, *35*, L10109, doi:10.1029/2008GL033875.

Lei, J., J. P. Thayer, J. M. Forbes, Q. Wu, C. She, W. Wan, and W. Wang (2008b), Ionosphere response to solar wind high-speed streams, *Geophys. Res. Lett.*, *35*, L19105, doi:10.1029/2008GL035208.

Lei, J., J. P. Thayer, W. Wang, and R. L. McPherron (2011), Impact of CIR storms on thermosphere density variability during the solar minimum of 2008, *Sol. Phys.*, *274*, 427–437, doi:10.1007/s11207-010-9563-y.

Ma, T.-Z., and R. W. Schunk (1995), Effect of polar cap patches on the polar thermosphere, *J. Geophys. Res.*, *100*(A10), 19,701–19,713, doi:10.1029/95JA01122.

Ma, T.-Z., and Schunk, R. W. (2001), The effects of multiple propagating plasma patches on the polar thermosphere, *J. Atmos. Sol. Terr. Phys.*, *63*, 355–366, doi:10.1016/S1364-6826(00)00181-4.

Mlynczak, M. G., F. J. Martin-Torres, C. J. Mertens, B. T. Marshall, R. E. Thompson, J. U. Kozyra, E. E. Remsberg, L. L. Gordley, J. M. Russel, and T. Woods (2008), Solar-terrestrial coupling evidenced by periodic behavior in geomagnetic indexes and the infrared energy budget of the thermosphere, *Geophys. Res. Lett.*, *35*, L05808, doi:10.1029/2007GL032620.

Pedatella, N. M., J. Lei, J. P. Thayer, and J. M. Forbes (2010), Ionosphere response to recurrent geomagnetic activity: Local time dependency, *J. Geophys. Res., 115, A02301, doi:10.1029/2009JA014712.*

Picone, J. M., A. E. Hedin, D. P. Drob, and A. C. Aikin (2002), NRLMSISE-00 empirical model of the atmosphere: Statistical comparisons and scientific issues, *J. Geophys. Res.*, *107*(A12), 1468, doi:10.1029/2002JA009430.

Qian, L., S. C. Solomon, and M. G. Mlynczak (2010), Model simulation of thermospheric response to recurrent geomagnetic forcing, *J. Geophys. Res.*, *115*, A10301, doi:10.1029/2010JA015309.

Rich, F., and M. Hairston (1994), Large-scale convection patterns observed by DMSP, *J. Geophys. Res.*, *99*, 3827–3844, doi:10.1029/93JA03296.

Roble, R. G., and E. C. Ridley (1987), An auroral model for the NCAR thermospheric general circulation model (TGCM), *Ann. Geophys., Ser. A*, *5*, 369–382.

Schunk, R. W. (1988), The polar wind, in *Modeling Magnetospheric Plasma*, *Geophys. Monogr. Ser.*, vol. 44, edited by T. M. Moore and J. H. Waite, pp. 219–228, AGU, Washington, D. C., doi:10.1029/GM044p0219

Schunk, R. W., and H. G. Demars (2003), Effect of equatorial plasma bubbles on the thermosphere, *J. Geophys. Res.*, *108*(A6), 1245, doi:10.1029/2002JA009690.

Schunk, R. W., L. Gardner, L. Scherliess, D. C. Thompson, and J. J. Sojka (2008), Effect of lower atmospheric waves on the ionosphere and thermosphere, in *Proceedings of the 2008 Ionospheric Effects Symposium*, pp. 300–307, Natl. Tech. Inf. Serv., Springfield, Va.

Sojka, J. J., R. W. Schunk, T. van Eyken, J. Kelly, C. Heinselman, and M. McCready (2007), Ionospheric challenges of the International Polar Year, *Eos Trans. AGU*, *88*(15), 171, doi:10.1029/2007EO150003.

Sojka, J. J., M. J. Nicolls, C. J. Heinselman, and J. D. Kelly (2009a), The PFISR IPY observations of ionospheric climate and weather, *J. Atmos. Sol. Terr. Phys.*, *71*, 771–785, doi:10.1016/j.jastp.2009.01.001.

Sojka, J. J., R. L. McPherron, A. P. van Eyken, M. J. Nicolls, C. J. Heinselman, and J. D. Kelly (2009b), Observations of ionospheric heating during the passage of solar coronal hole fast streams, *Geophys. Res. Lett.*, *36*, L19105, doi:10.1029/2009GL039064.

Temmer, M., B. Vrsnak, and A. M. Veronig (2007), Periodic appearance of coronal holes and the related variation of solar wind parameters, *Sol. Phys.*, *241*, 371–383, doi:10.1007/s11207-007-0336-1.

Thayer, J. P., J. Lei, J. M. Forbes, E. K. Sutton, and R. S. Nerem (2008), Thermospheric density oscillations due to periodic solar wind high-speed streams, *J. Geophys. Res.*, *113*, A06307, doi:10.1029/2008JA013190.

Torr, M. R., D. G. Torr, and H. E. Hinteregger (1980), Solar flux variability in the Schumann-Runge continuum as a function of solar cycle 21, *J. Geophys. Res.*, *85*, 6063–6068, doi:10.1029/JA085iA11p06063.

Tulasi Ram, S., C. H. Liu, and S.-Y. Su (2010), Periodic solar wind forcing due to recurrent coronal holes during 1996–2009 and its impact on Earth's geomagnetic and ionospheric properties during the extreme solar minimum, *J. Geophys. Res.*, *115*, A12340, doi:10.1029/2010JA015800.

Volland, H. (1975), Models of the global electric fields within the magnetosphere, *Ann. Geophys.*, *31*, 159–173.

Zalesak, S. T. (1979), Fully multi-dimensional flux-corrected transport algorithms for fluids, *J. Comput. Phys.*, *31*, 335–362, doi:10.1016/0021-9991(79)90051-2.